THE JOURNAL OF PHYSICAL CHEMISTRY A

Article

Structural, Optical and Electronic Properties of Wide Bandgap Perovskites: Experimental & Theoretical Investigation

Naresh Kumar Kumawat, Madhvendra Nath Tripathi, Umesh V. Waghmare, and Dinesh Kabra

J. Phys. Chem. A, **Just Accepted Manuscript** • DOI: 10.1021/acs.jpca.6b04138 • Publication Date (Web): 20 May 2016

Structural, Optical and Electronic Properties of Wide Bandgap Perovskites: Experimental & Theoretical Investigations

Naresh K. Kumawat[1], Madhvendra Nath Tripathi[2], Umesh Waghmare[3], Dinesh Kabra[*1]*

[1]Department of Physics, Indian Institute of Technology Bombay (IITB), Powai, Mumbai-400076, India

[2]Department of Pure & Applied Physics, Guru Ghasidas Vishwavidyalaya (Central University), Koni, Bilashpur-495009, India

[3]Thematic Unit for Computational Materials Science, Jawaharlal Nehru Centre for Advanced Scientific Research, Jakkur, Bangalore-560064, India

AUTHOR INFORMATION

Corresponding Author *To whom correspondence should be addressed

*E-mail: dkabra@iitb.ac.in

(Telephone Number +91-22 -2576 7589)

Abstract

Wide bandgap hybrid halide perovskites based on bromine and chlorine halide anions have emerged as potential candidates for various optoelectronic devices. However, these materials are relatively less explored than the iodine based perovskites for microscopic details. We present experiment and first-principles calculations to understand the structural, optical and electronic structure of wide bandgap $CH_3NH_3Pb(Br_{1-x}Cl_x)_3$ (x = 0, 0.33, 0.66 and 1) 3D hybrid perovskite materials. We substituted Br^- with Cl^- in order to tune the bandgap from 2.4 eV (green emissive) to 3.2 eV (blue (UV) emissive) of these materials. We correlate our experimental results with first-principles theory and provide an insight into important parameters like; lattice constants, electronic structure, excitonic binding energy (E_X), dielectric constant and reduced effective mass (μ_r) of charge carriers in these perovskite semiconductors. Electronic structure calculations reveal that electronic properties are mainly governed by Pb *6p* and halide *p* orbitals. Our estimates of E_X within a hydrogen model suggest that increase in E_X by increasing the Cl^- (chlorine) concentration is mainly due to decrease in the dielectric constant with *x* and almost constant value of μ_r close to the range of $0.07m_e$.

1. INTRODUCTION

Organic-inorganic 3D-metal halide perovskite materials have become potential candidates for use in optoelectronic devices, with solar cell efficiency boost up from 3% to 20.1%[1-5], efficient electroluminescence from visible to NIR range, lasers and photo-detector applications.[6-10] These compounds occur in the standard ABX_3 perovskite structure, where A, B & X are organic cations e.g. $CH_3NH_3^+$, divalent metal cation e.g. Pb^{+2}, Sn^{+2}, and halogen anion e.g. Cl^-, Br^-, I^-, respectively. These materials are of low cost due to their low temperature solution processing thin-film deposition techniques, which provide a polycrystalline films with high charge carrier-mobility.[11-15] So far, most of the fundamental studies of devices have focused on iodine based hybrid perovskites because of high solar cell efficiency even in the planar cell geometry. However, whether it is for lighting/display or tandem solar cells wider band gap perovskites are equally important,[16,17] and fundamental studies of these wide bandgap perovskites are necessary to understanding the influence of halide ions on various semiconductor material parameters apart from most the studied bandgap. The other important parameters include shape or dispersion of band structure which relates to the effective masses of charge carriers, dielectric constants and exciton binding energy (E_X). A good understanding of these parameters not only provides the insight into physics of devices based on these compounds, but also opens a scope for development of new compounds (with different metal ion or molecular ion) from a similar ABX_3 family.

In this paper, we compare our experimentally observed band gap and exciton binding energies with the values obtained from DFT calculations. The DFT investigations of these halide pervoskite compositions provide useful insight into their electronic structure as a function of composition, identifying the specific material

parameters that are responsible for changes in the exciton binding energy. Our work provides an understanding of these optoelectronic materials and also provides a guideline to design new materials with desired properties in similar family of halide perovskite materials.

2. COMPUTATION DETAILS

In this manuscript, our focus is to get an insight of electronic structure using first-principles on $AB(Br_{1-X}Cl_X)_3$ perovskites, which are potential blue light emitting materials for lighting/display devices. Our first-principles calculations are based on density functional theory (DFT), as implemented in the PWscf package.[18] The calculations were performed using Perdew–Burke–Ernzerhof (PBE) exchange-correlation functional[19] within a generalized gradient approximation (GGA).[20] We focus on the pseudo-cubic phase of mixed halide material with $AB(Br_{1-x}Cl_x)_3$; x = 0, 0.33, 0.66, and 1. We used plane-wave basis sets to represent wave functions and density of valence electrons, and scalar relativistic ultrasoft pseudo-potentials[21] to describe the interaction between ions and valence electrons: N and C 2s, 2p; H 1s; Pb 5d, 6s, 6p; Br 4s, 4p; and Cl 3s, 3p. Energy cutoffs of 30 R_y and 270 R_y were used to truncate the plane-wave basis sets used in representation of wave functions and density respectively. We use 8x8x8 k-point meshe to sample integrations over the Brillouin zone to obtain energies and electronic structure of different mixed halide compositions. We optimized the atomic geometry through total energy minimization using the Hellmann-Feynman forces.[22] Such materials can sustain macroscopic electric fields, which couple with vibrations described by Born effective charges. These and electronic dielectric constants were determined using DFT linear-response as implemented in Quantum Espresso. The theoretical estimates of

dielectric constants and reduced effective mass are used to determine the E_X for these materials.

3. EXPERIMENTAL SECTION

For perovskite thin film deposition, we have followed method described earlier.[14] We prepared perovskite solution of $ABBr_3$ and $ABCl_3$ using CH_3NH_3Br and CH_3NH_3Cl with $PbBr_2$ and $PbCl_2$ with 1:1 molar solution in DMSO, respectively. We mixed the perovskite in volumetric ratio of $ABCl_3/ABBr_3$ to tune the structural and optical property of $AB(Br_{1-x}Cl_x)_3$ perovskite system. Perovskite thin film deposited inside the N_2 filled glove box by 2000 rpm for 30 second on cleaned substrates. Structural analysis is done using HRXRD, (Regaku HRXRD SmartLab; $Cu_{K\alpha}$ =1.54 Å) and optical studies are carried out using Perkin Elmer Lambda 900 absorbance and FluoroMAX photoluminescence spectrometer. Morphological and element analysis is done using FESEM in EDX mode.

4. RESULTS AND DISCUSSION

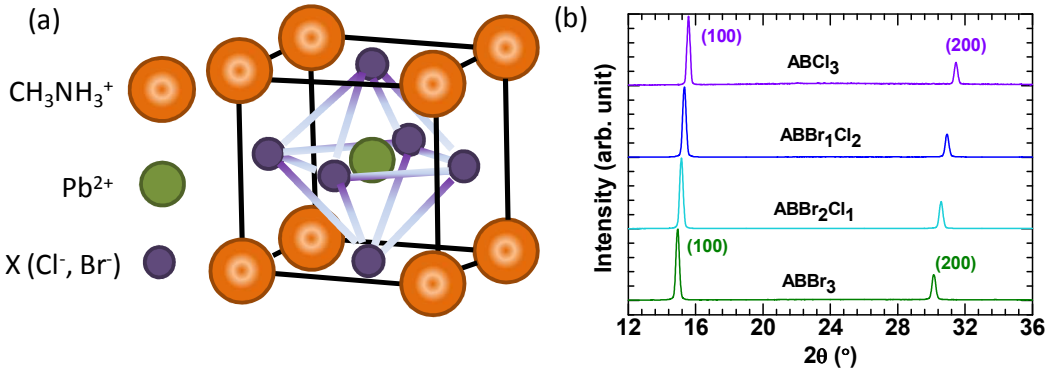

Figure 1: (a) Typical crystal Structure of organic-Inorganic perovskite materials ($AB(Br_{1-x}Cl_x)_3$); wherein $CH_3NH_3^+$, Pb^{2+} and X^- occupy the corner (orange), body centered (green) and face centered (violet) position, respectively **(b)** X-ray diffraction pattern of $AB(Br_{1-x}Cl_x)_3$ perovskite film (x = 0, 0.33, 0.66 and 1) on PEDOT:PSS/glass substrate.

We have performed experimental structural and optical characterization of $AB(Br_{1-X}Cl_X)_3$ perovskite semiconductor films. **Figure 1 (a)** shows crystal structure of metal halide perovskite wherein $CH_3NH_3^+$, Pb^{2+} and X^- (Cl^-, Br^-) occupy corner, body and face centred sites, respectively. In the crystal structure, PbI_6 cage plays an important role in determining the electronic properties of a perovskite material. Here, we tune the structural properties of $AB(Br_{1-x}Cl_x)_3$ wide band gap perovskite material by mixing the $ABBr_3$ in $ABCl_3$. $ABCl_3$ and $ABBr_3$ both have cubic crystal structure at room temperature. Hence, $AB(Br_{1-x}Cl_x)_3$ also has a cubic crystal structure at room temperature.[14,23] **Figure 1 (b)** shows x-ray diffraction pattern for ($AB(Br_{1-x}Cl_x)_3$; x=0,0.33, 0.66 and 1) perovskite materials deposited on PEDOT:PSS/glass substrate after annealing wherein we could change crystal structure with Br/Cl ratio. Diffraction angle and (hkl) values are matched with reported values (see in **Figure S1** & **Table S1**).[24,25] Metal halide perovskite materials are long ordered crystalline materials, and we observe from Figure 1 (b) that XRD peaks shift towards higher diffraction angles with increase in Cl^- concentration in $AB(Br_{1-x}Cl_x)_3$ and this is because of smaller atomic size of Cl^-.[26] The XRD peaks are quite sharp, thus these materials are good crystalline; narrow XRD peak is an indication of quality of materials in terms of fewer grain boundary defects. XRD peaks are found to be slightly broader (FWHM) for mixed halide ($AB(Br_{1-x}Cl_x)_3$) cases than the end-member pure single halides ($ABBr_3$ & $ABCl_3$) (see in **Figure 2d**). Compositional analysis was performed using FESEM (field emission scanning electron microscopy) in EDX mode (see in **Figure S2**). For the compositional values (x = 0, 0.33, 0.66, and 1), the lattice parameters satisfy the Vegard's law of a linear relationship between them. This suggests that $AB(Br_{1-x}Cl_x)_3$ perovskite film has cubic crystal structure in all four

compositions and lattice parameter decreases monotonically with increase in chlorine content (see in **Figure S3**).[14,26]

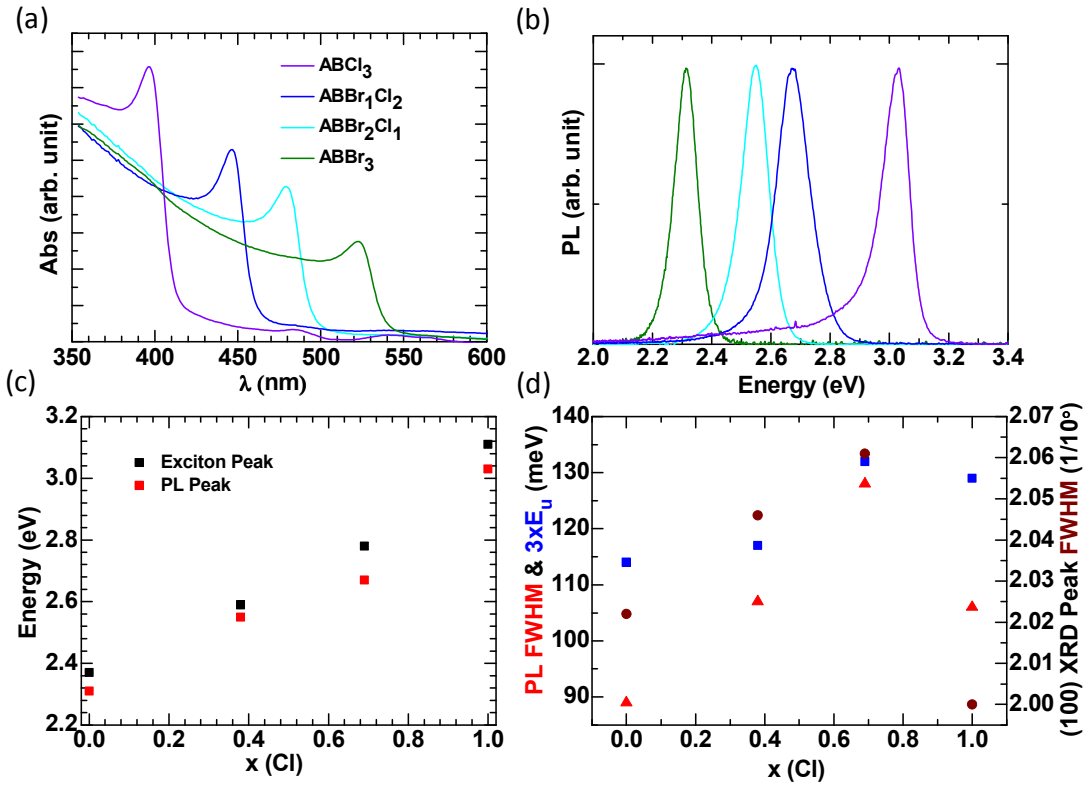

Figure 2: (a) Absorbance spectra of $AB(Br_{1-x}Cl_x)_3$ (x = 0, 0.33, 0.66 and 1) on PEDOT:PSS/glass substrate after annealing **(b)** Photoluminescence (PL) spectra of $AB(Br_{1-x}Cl_x)_3$ (x=0, 0.33, 0.66 and 1) at 355 nm excitation wavelength **(c)** Excitonic peak and PL peak vs composition curve which shows excitonic peak are blue shifted from PL peak **(d)** FWHM of PL peak, Urbach energy and FWHM of XRD peak vs Chlorine contents in $AB(Br_{(1-x)}Cl_x)_3$ film.

Table 1: Experimental and theoretically calculated bandgap and lattice parameter values for various perovskites $AB(Br_{1-x}Cl_x)_3$.

Perovskites	Lattice Parameter (Å)		Band gap (eV)	
	Calculated	Experimental	Calculated	Experimental
$ABBr_3$	6.05	5.95	2.17	2.42
$ABBr_2Cl$	5.98	5.83	2.30	2.59
$ABBrCl_2$	5.91	5.75	2.52	2.82
$ABCl_3$	5.80	5.66	2.61	3.16

We investigated optical properties of $AB(Br_{1-X}Cl_X)_3$ perovskite films using steady state absorption and photoluminescence spectrum studies. **Figure 2** (a) shows absorbance spectra for $AB(Br_{1-x}Cl_x)_3$ film with x=0, 0.33, 0.66, 1. From absorbance spectral measurements, we observe that the band-edge of the spectrum is dominated by an excitonic peak at room temperature, and it gets sharper with increase in chlorine content in the perovskite along with a blue shift in the band-edge. Steeper band-edges suggest that $AB(Br_{1-x}Cl_x)_3$ are ordered in nature and are direct bandgap semiconductors. However, Tauc formula is not the correct method for determination of electronic bandgap of these wide bandgap perovskite semiconductors, as the excitonic absorption dominates at band-edge and influence the oscillator strength of inter-band transitions. We calculate electronic bandgap (E_g), E_X and excitonic peak position from absorbance spectra using Sommerfield theory of Wannier exciton.[14,27] E_g and E_X are given in **Table 1** & **Table 2**. We also fit the tail part of absorbance spectra to calculated Urbach energy (see in **Figure S4**), which is

found to be lower for Single halide and slightly higher for mixed halide based perovskite films. This suggests that the measured disorder is probably due to more grain boundaries (domain size α 1/XRD's FWHM) in the case of mixed halide film that is in agreement with our structural studies (see in Figure 2d). **Figure 2(b)** shows photoluminescence spectra of all the four compounds. We observed a blue shift in the PL peak and full width at half maxima (FWHM ~ 110 ± 15 meV) of PL peak shows almost similar behavior like Urbach & FWHM of XRD peak (See Figure 2d, Figure S4 and Table S2) with respect to change in composition. PL peak is red shifted from excitonic peak by ~110 meV and both follow same trend see in **Figure 2c**. This redshift can be attributed to spectral diffusion of the excited state, which depends on FWHM of exciton absorption peak and temperature.

Table 2: Average reduced effective mass (μ_r), dielectric constant (ε_r) and exciton binding energy (E_X) values calculated by DFT model.

Perovskites	R-M		R-G		μ_1 R-M	μ_2 R-G	$\mu_r = (\mu_1+\mu_2)/2$	ε_r	Calc. E_X (meV)	Exp. E_X (meV)
	m_e	m_h	m_e	m_h						
$ABBr_3$	0.20	0.16	0.12	0.11	0.089	0.057	0.073	4.67	45	45
$ABBr_2Cl$	0.22	0.21	0.10	0.12	0.107	0.052	0.079	4.28	58	53
$ABBrCl_2$	0.20	0.17	0.12	0.11	0.091	0.057	0.074	3.96	64	58
$ABCl_3$	0.16	0.15	0.12	0.10	0.085	0.057	0.071	3.76	68	64

Experimental observations of the changes in optoelectronic properties with change in the halide anion content presented above augur well for the tenability of

hybrid perovskites. However, it is not quite clear how the halide content affects microscopic and macroscopic parameters, like carrier effective mass, dielectric constant, density of states and band structure of each semiconductor material, and needs more insightful theoretical investigations. First, we describe structural properties of these films. The standard DFT-GGA calculations usually provide geometrical structure and relative stability in good agreement with experimental data.[28] Our theoretical results for the lattice parameters of mixed halide are summarised in Table 1. The calculated lattice parameters for the pseudo cubic structured[17] composition $AB(Br_{1-x}Cl_x)_3$ are 6.05 Å(5.95 Å), 5.98 Å (5.83 Å), 5.90 Å (5.75 Å), and 5.82 Å (5.66 Å) for x = 0, 0.33, 0.66, and 1 respectively, which are slightly larger than experimental values within an acceptable limit (about 1 % overestimation is typical of GGA calculations). The standard GGA-PBE is well known to provide the geometrical structures and relative stabilities for the perovskites. However, for $CH_3NH_3PbI_3$, the overestimation of GGA(PBE)-calculated lattice parameters was attributed to the neglect of van der Waals interactions between the cationic CH_3NH_3 and anionic [Pb–I] frameworks.[29,30] The inclusion of vander Waals interactions in DFT may improve the calculated lattice parameters as reported earlier,[8,13] however, the electrostatic interaction is expected due to interaction of the cationic organic molecules with the anionic inorganic matrix resulting ionic nature of these compounds which are well described in DFT-GGA.[28] In this regard, the current halide perovskites are expected to be different from organic materials for which van der Waals force dominates the intermolecular interactions. In a very recent paper,[31] the lattice parameters and atomic positions of Pb- and Sn-based perovskites were fully optimized using the Perdew-Burke-Ernzerhof (PBE) functional within the generalized gradient approximation (GGA). In the present calculation, the optimised

lattice parameters obtained within standard GGA-PBE agree within the typical GGA errors with experimental results.[14,25,26] In any case, to evaluate the impact of this small error on electronic properties, we determined the band-gap at experimental lattice constant, and find that it changes by only 0.12 eV. The band-gap values of 2.17 (2.05) eV were obtained for $ABBr_3$ for optimised (experimental) lattice constant values of 6.05 Å (5.95 Å), however, band structure remains same.

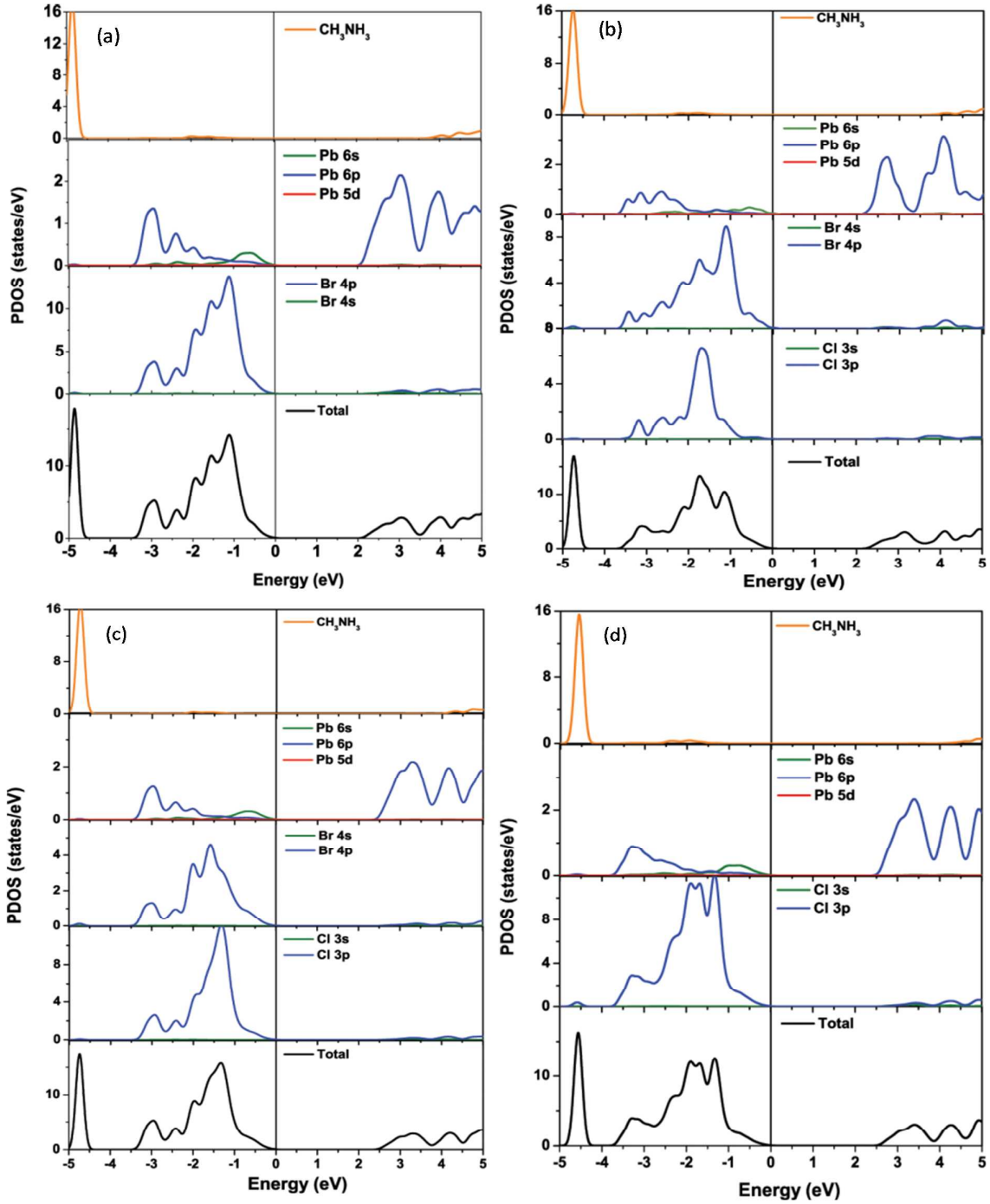

Figure 3: PDOS of $AB(Br_{(1-x)}Cl_x)_3$ for **(a)** x=0, **(b)** x=0.33, **(c)** x=0.66 and **(d)** x=1.The zero is set at top of valence band.

Thus, effects of errors in lattice constants would not alter our conclusions on anion-dependent exciton properties studied here. The structural data suggests the preferential occupation of Cl^- ion at the apical site, which is consistent with the previous reports.[32,33] The lattice parameter decreases as the chlorine content increases because of its smaller radius as compared to bromine. A smaller chlorine anion has a smaller cavity with a slight structural destabilisation as reflected in energetics and increase in the band gap. The calculated band gaps with DFT-GGA are presented in Table 1, which agree well with experimental values.[14] Typically, the standard DFT-GGA calculations underestimate the band gap. In the present cases, the GGA-DFT estimates of gaps are close to experimental values because of cancellation of errors associated with neglect of (a) spin-orbit coupling (SOC) which causes reduction in the gap, and (b) self-interaction corrections which result in increase in the gap.[28] Since, we are interested in trends and changes in electronic properties with Cl concentration (Table 1 & Figure S5), it is reliable and cost-effective to continue the calculations with GGA-DFT.

The partial density of electronic states of $AB(Br_{1-x}Cl_x)_3$ for x=0, 0.33, 0.66, and 1 are presented in **Figure 3 (a-d)**. The width of uppermost valence band is 3.5 eV for x = 0. The main contribution from states of $CH_3NH_3^+$ comes around 5.0 eV deep below the VBM and it does not play a significant role in optical and electronic response of material similar to ABI_3.[34] The organic cations do not contribute to VBM and CBM which are responsible for conductivity however they maintain overall charge neutrality[35] and structural stability.

The states at the valence band maximum (VBM) originate mainly from the strong bonding and anti-bonding states of the Br *4p* and Pb *6s* orbitals, hybridization of which is responsible for dispersive nature of uppermost valence band. On the other

hand, the bottom of valence band comprises mainly of the states of Br and Pb *p* orbitals. The dispersive nature of upper valence band gives the smaller hole effective

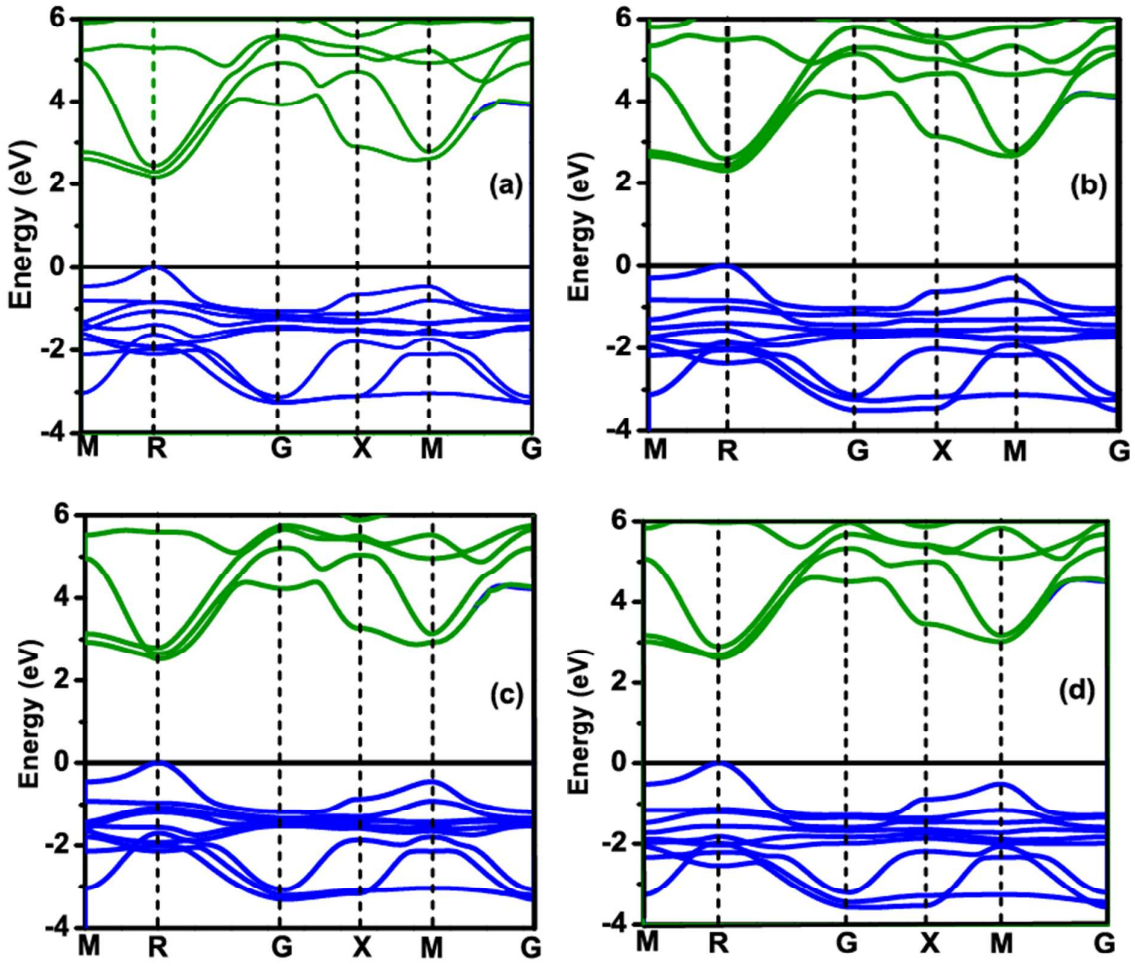

Figure 4: Electronic band structure of $AB(Br_{1-x}Cl_x)_3$ for **(a)** x=0, **(b)** x=0.33, **(c)** x=0.66 and **(d)** x=1.The zero is set at top of valence band.

mass comparable with electron effective mass as shown in Table 2 and consistent with earlier report.[36] The small effective mass results in high carrier mobility which is an important criterion for the good power efficiency of photovoltaic materials. The conduction band minimum (CBM) originates from Pb 6p orbitals having negligible coupling with Br 4p orbitals and shows a weakly bonding state between Pb 6s and Br 4p orbitals.[37] The addition of chlorine introduces Cl 3p states in the uppermost

valence band whereas the valence band edge is still mainly Br 4p states for x = 0, and 0.33, mixed contribution from Br 4p and Cl 3p in x = 0.66, and comes from Cl 3p in x = 1. In the deep valence band, the change in the number of peaks is evident ~ -13.5 eV (see in **Figure S6**) due to change in contributions of s orbitals of halide atoms. However, the Pb 6p contribution at CBM remains unchanged at all compositions.

In perovskite $ABBr_3$, the Pb and CH_3NH_3 donate two and one electron respectively to three Br ions forming a direct band gap of 2.17 eV between unoccupied Pb p orbitals and occupied Br p orbitals leading to high efficient optical absorption. The CH_3NH_3 has no covalent bonding with the Pb-Br framework and therefore does not create any additional gap states. All compositions of x between 0 and 1 have direct band gaps (see in **Figure 4**) and both the VBM and CBM were found to be located at R-point of Brillouin zone. The average carrier velocity in $AB(Br_{1-x}Cl_x)_3$ for x = 0.33-1.0 should be lower than that in $ABBr_3$ due to more localised Cl *3p* states than Br *4p* states.[38] The band gap increases when bromine is replaced with chlorine atom, which is consistent with previous report.[39] The effective masses are relatively very small. The effective mass of a hole at the VBM is lower than that of an electron at CBM and the calculated values are consistent with the previous report for x = 0 and x = 1 end-members.[40] The reduced effective mass is calculated using

$$\frac{1}{\mu_r} = \frac{1}{m_e} + \frac{1}{m_h} \quad (1)$$

Wherein, m_e and m_h are electron and hole effective masses, respectively.

The reduced effective mass of carriers was calculated as a function of x, and then used in finding average values of the reduced masses (see in Table 2). Reduced effective mass of these materials is found to be in a small range near 0.07 m_e, which are in very good agreement with recent experimental studies by Di *et al*[41] and Galkowski *et al.*[42]

The addition of chlorine increases the band gap, and hence the onset of absorption moves towards higher energy. However, the onset of optical absorption is dominated by the excitonic effects. The coulomb field of excitons influences the absorption at the band edges.[14] The E_X is given

$$E_X = (\mu_r/{\varepsilon_r}^2)13.6\ eV \qquad (2)$$

Where, μ_r is the reduced effective mass, and ε_r is the optical or electronic dielectric constant (square of refractive index).

The theoretical estimates of dielectric constants for different compositions obtained using DFT-linear response are shown in Table 2**.** Due to pseudo-cubic lattice structural symmetry, the dielectric response of the hybrid materials is anisotropic and we use the average values of dielectric constant for different compositions in further analysis. The dielectric constant decreases with increasing concentration of chlorine in composition. It was notes earlier that dielectric constant for $ABBr_3$ (4.8) is smaller than ABI_3 (6.5),[43] and it was explained with argument that the lower dielectric constant in $ABBr_3$, comes from its larger band gap, and it results in larger exciton binding energy.[44] Moreover, one possibility is that each A ($CH_3NH_3^+$) cation is located in a cage formed by the 12 nearest halogen atoms in the ABX_3 hybrid perovskites. The size of this cage reduces when bromine is substituted with the

chlorine leading to reduced polarizability, and a drop in the dielectric constant, and subsequent increases in E_X.

5. CONCLUSION

In conclusion, we presented a combined experimental and theoretical analysis of the structural and optoelectronic properties of wide bandgap perovskite materials, which have been shown to be potential candidates for use in optoelectronic devices in the UV-Vis range of electromagnetic spectrum. Our comparative analysis of experimental and theoretical results with reveals that a reduction in the lattice constant with increasing concentration of smaller Cl^- ion at Br^- site leads to increase in bandgap ($E_g \alpha 1$/lattice constant) and reduction in the dielectric constant. We show that anionic substitution results in changes in density of states, bandgap and dielectric constant of materials. We find a reasonably good accuracy in estimation of effective reduced mass (0.07 m_e) and eventually a quantitative estimation of E_X in the range from 45 to 65 meV. E_X separately determined from Wannier-exciton model and a fit to absorption spectrum is in good agreement with calculated values. Overall, our work provides insights into composition dependent structural and optoelectronic properties of these materials, and should guide design of new materials with desired properties in halide based perovskite materials.

Supporting Information Available:

The Supporting Information is available free of charge on the ACS Publications website. Figure S1-S6.

Funding:

This work is partially supported by the IITB Seed grant (12IRCCSG044) and Department of Science & Technology (DST/TM/SERI/FR/186(G)), India. We also acknowledge support of Centre of Excellence in Nanoelectronics (CEN) for deposition facility and National Centre for Photovoltaic Research and Education (NCPRE) for characterization.

Acknowledgement:

We thank Prof. Anil Kumar from Chem. IITB-Mumbai for providing synthesis facility and Prof. K. L. Narasimhan, EE IITB-Mumbai for useful discussion about exciton model. Thanks to Thematic Unit of Excellence on Computational Material Science (TUE-CMS), Jawaharlal Nehru Centre for Advanced Scientific Research (JNCASR), Bangalore, for providing computational facility.

Reference

(1) Kojima, A; Teshima, K; Shirai, Y; Miyasaka, T. Organometal Halide Perovskites as Visible-Light Sensitizers for Photovoltaic Cells. *J. Am. Chem. Soc.* **2009**, *131*, 6050–6051.

(2) Lee, M. M.; Teuscher, J.; Miyasaka, T.; Murakami, T. N.; Snaith, H. J. Efficient Hybrid Solar Cells Based on Meso-Superstructured Organometal Halide Perovskites. *Science* **2012**, *338*, 643-647.

(3) Burschka, J.; Pellet, N.; Moon, S.-J.; Baker, R. H.; Gao, P.; Nazeeruddin, M. K.; Gratzel, M. Sequential Deposition as a Route to High-Performance Perovskite-Sensitized Solar Cells. *Nature* **2013**, *499*, 316-319.

(4) Liu, M.; Johnston, M. B.; Snaith, H. J. Efficient Planar Heterojunction Perovskite Solar Cells by Vapour Deposition. *Nature* **2013**, *501*, 395–398.

(5) Zhou, H.; Chen, Q.; Li, G.; Luo, S.; Song, T.-B.; Duan, H.-S.; Hong, Z.; You, J.; Liu, Y.; Yang Y. Interface Engineering of Highly Efficient Perovskite Solar Cells. *Science* **2014**, *345*, 542-546.

(6) Deschler, F.; Price, M.; Pathak, S.; Klintberg, L. E.; Jarausch, D. D.; Higler, R.; Huttner, S.; Leijtens, T.; Stranks, S. D.; Snaith, H. J.; Atature, M.; Phillips, R. T.; Friend, R. H. High Photoluminescence Efficiency and Optically Pumped Lasing in Solution-Processed Mixed Halide Perovskite Semiconductors. *J. Phys. Chem. Lett.* **2014**, *5*, 1421–1426.

(7) Xing, G.; Mathews, N.; Lim, S. S.; Yantara, N.; Liu1, X.; Sabba, D.; Gratzel, M.; Mhaisalkar, S.; Sum, T. C. Low-Temperature Solution Processed Wavelength-Tunable Perovskites for Lasing. *Nat. Mater.* **2014**, *13*, 476-480.

(8) Zhu, H.; Fu, Y.; Meng, F.; Wu, X.; Gong, Z.; Ding, Q.; Gustafsson, M. V.; Trinh, M. T., Jin, S.; Zhu, X.-Y. Lead Halide Perovskite Nanowire Lasers with Low Lasing Thresholds and High Quality Factors. *Nat. Mater.* **2015**, *14*, 636–643.

(9) Stranks, S. D.; Burlakov, V. M.; Leijtens, T.; Ball, J. M.; Goriely, A.; Snaith, H. J. Recombination Kinetics in Organic-Inorganic Perovskites: Excitons, Free Charge, and Subgap States. *Phys. Rev. A*. **2014**, *2*, 034007.

(10) Chin, X. Y.; Cortecchia, D.; Yin, J.; Bruno, A.; Soci, C. Lead Iodide Perovskite Light-Emitting Field-Effect Transistor. *Nat. Commun*. **2015**, *6*, 7383, 1-7.

(11) Su, L.; Zhao, Z. X.; Li, H. Y.; Yuan, J.; Wang, Z. L.; Cao, G. Z.; Zhu, G. High-Performance Organolead Halide Perovskite-Based Self-Powered Triboelectric Photodetector. *ACS Nano* **2015**, *9*, 11310–11316.

(12) Yakunin, S.; Sytnyk, M.; Kriegner, D.; Shrestha, S.; Richter, M.; Matt, G. J.; Azimi, H.; Brabec, C. J.; Stangl, J.; Kovalenko, M. V.; Heiss, W. Detection of X-ray Photons by Solution-Processed Lead Halide Perovskites. *Nat. Photonics* **2015**, *9*, 444-449.

(13) Kumawat, N. K., Dey, A.; Narasimhan, K. L.; Kabra, D. Near Infrared to Visible Electroluminescent Diodes Based on Organometallic Halide Perovskites: Structural and Optical Investigation. *ACS Photonics* **2015**, *2*, 349−354.

(14) Kumawat, N. K.; Dey, A.; Kumar, A.; Gopinathan, S. P.; Narasimhan, K. L.; Kabra, D. Band Gap Tuning of $CH_3NH_3Pb(Br_{1-x}Cl_x)_3$ Hybrid Perovskite for Blue Electroluminescence. *ACS Appl. Mater. Interfaces* **2015**, *7*, 13119−13124.

(15) Cho, H.; Jeong, S.-H.; Park, M.-H.; Kim, Y.-H.; Wolf, C.; Lee, C.-L.; Heo, J. H.; Sadhanala, A.; Myoung, N.; Yoo, S.; Im, S. H.; Friend, R. H.; Lee, T.-W. Overcoming

the Electroluminescence Efficiency Limitations of Perovskite Light-Emitting Diodes. *Science* **2015**, *350*, 1222-1225.

(16) Bailieand, C. D.; McGehee, M. D. High-Efficiency Tandem Perovskite Solar Cells. *MRS Bulletin* August, **2015**.

(17) Werner, J. M.; Weng, C.-H.; Walter, A.; Fesquet, L.; Seif, J. P.; Wolf, S. D.; Niesen, B.; Ballif, C. Efficient Monolithic Perovskite/Silicon Tandem Solar Cell with Cell Area >1 cm^2. *J. Phys. Chem. Lett.* **2016**, *7*, 161–166.

(18) Giannozzi, P.; Baroni, S.; Bonini, N.; Calandra, M.; Car, R.; Cavazzoni, C.; Ceresoli, D.; Guido, L. C.; Cococcioni, M.; Dabo, I. QUANTUM ESPRESSO: a Modular and Open-Source Software Project for Quantum Simulations of Materials. *J. Phys. Condens. Matter.* **2009**, *21*, 395502.

(19) Perdew, J. P.; Burke, K.; Ernzerhof, M. Generalized Gradient Approximation Made Simple. *Phys. Rev. Lett.* **1996**, *77*, 3865−3868.

(20) Wang, Y.; Perdew, J. P. Spin Scaling of the Electron-Gas Correlation Energy in the High-Density Limit. *Phys. Rev. B* **1991**, *43*, 8911-8916.

(21) Vanderbilt, D. Soft Self-Consistent Pseudopotentials in a Generalized Eigenvalue Formalism. *Phys. Rev. B* **1990**, *41*, 7892-7895.

(22) Feynman, R. P. Forces in Molecules. *Phys. Rev.* **1939**, *56*, 340-343.

(23) Kitazawa, N; Watanabe, Y; Nakamura, Y. Optical Properties of $CH_3NH_3PbX_3$ (X=halogen) and Their Mixed-Halide Crystals, *J. of Mater. Sci.* **2002**, 37, 3585.

(24) Sadhanala, A.; Ahmad, S.; Zhao, B.; Giesbrecht, N.; Pearce, P. M.; Deschler, F.; Hoye, R. L. Z.; Godel, K. C.; Bein, T.; Docampo, P.; Dutton, S. E.; De Volder, M.

F. L.; Friend, R. H. Blue-Green Color Tunable Solution ProcessableOrganolead Chloride−Bromide Mixed Halide Perovskites for Optoelectronic Applications. *Nano Lett.* **2015**, *15*, 6095–6101.

(25) Comin, R.; Walters, G.; Thibau, E. S.; Voznyy, O.; Lub, Z.-H.; Sargent, E. H. Structural, Optical, and Electronic Studies of Wide-Bandgap Lead Halide Perovskites. *J. Mater. Chem. C* **2015**, *3*, 8839-8843.

(26) Noh, J. H.; Im, S. H.; Heo, J. H.; Mandal, T. N.; Seok, S. Il Chemical Management for Colorful, Efficient, and Stable Inorganic–Organic Hybrid Nanostructured Solar Cells. *Nano Lett.* **2013**, *13*, 1764–1769.

(27) Elliott, R. Intensity of Optical Absorption by Excitons. *Physical Review* **1957**, *108*, 1384–1389.

(28) Mosconi, E.; Amat, A.; Nazeeruddin, M. K.; Gratzel, M.; Angelis, D. First-Principles Modeling of Mixed Halide Organometal Perovskites for Photovoltaic Applications. *J. Phys. Chem. C* **2013**, *117*, 13902-13913.

(29) Egger, D. A.; Kronik, L. Role of Dispersive Interactions in Determining Structural Properties of Organic−Inorganic Halide Perovskites: Insights from First Principles Calculations. *J. Phys. Chem. Lett.* **2014**, *5*, 2728–2733.

(30) Even, J; L. Pedesseau, L; Jancu, J.-M.; Katan, C. Importance of Spin-orbital coupling in hybrid organic/inorganic perovskites for photovoltaic applications. *J. Phys. Chem. Lett.* **2013**, *4*, 2999-3005.

(31) Zhao, T.; Shi, W.; Xi, J.; Wang, D.; Shuai, Z. Intrinsic and Extrinsic Charge Transport in $CH_3NH_3PbI_3$ Perovskites Predicted from First-Principles. *Sci. Rep.* **2016**, *6*, 19968.

(32) Zheng, F.; Takenaka, H.; Wang, F.; Koocher, N. Z.; Rappe, A. M. First-Principles Calculation of the Bulk Photovoltaic Effect in $CH_3NH_3PbI_3$ and $CH_3NH_3PbI_{3-x}Cl_x$. *J. Phys. Chem. Lett.* **2015**, *6*, 31-37.

(33) Kuo, Y.-K.; Liou, B.-T.; Yen, S.-H.; Chu, H.-Y. Vegard's Law Deviation in Lattice Constant and Band Gap Bowing Parameter of Zincblende $In_xGa_{1-x}N$. *Opt. Commun*. **2004**, *237*, 363-369.

(34) Motta, C.; Mellouhi, F. E.; Kais, S.; Tabet, N.; Alharbi, F.; Sanvito, S. Revealing the Role of Organic Cations in Hybrid Halide Perovskite $CH_3NH_3PbI_3$. *Nat. Commun.* **2015**, *6,* 7026.

(35) Borriello; Cantele, G.; Ninno, D. Ab Initio Investigation of Hybrid Organic-Inorganic Perovskites Based on Tin Halides. *Phys. Rev. B* **2008**, *77*, 235214.

(36) Yin, W.-J.; Shi, T.; Yan Y. Superior Photovoltaic Properties of Lead Halide Perovskites: Insights from First-Principles Theory. *J. Phys. Chem. C* **2015**, *119*, 5253-5264.

(37) Chang, Y. H.; Park, C. H. First-Principles Study of the Structural and the Electronic Properties of the Lead-Halide-Based Inorganic-Organic Perovskites $(CH_3NH_3)PbX_3$ and $CsPbX_3$ (X = Cl, Br, I). *J. of Korean Physical Society* **2004**, *44*, 889-893.

(38) Du, M. H.; Efficient Carrier Transport in Halide Perovskites: Theoretical Perspectives. *J. Mater.Chem. A* **2014**, *2*, 9091-9098.

(39) Umebayashi, T.; Asai, K.; Kondo, T.; Nakao, A. Electronic Structures of Lead Iodide Based Low-Dimensional Crystals. *Phys. Rev. B* **2003**, *67*, 155405.

(40) Umari, P.; Mosconi, E.; Angelis, F. D. Relativistic GW calculations on $CH_3NH_3PbI_3$ and $CH_3NH_3SnI_3$ Perovskites for Solar Cell Applications. *Sci. Rep.* **2014**, *4*, 4467.

(41) Di, D.; Musselman, K. P.; Li, G.; Sadhanala, A.; Ievskaya, Y.; Song, Q.; Tan, Z.-K.; Lai, M. L.; MacManus-Driscoll, J. L.; Greenham, N. C.; Friend, R. H. Size-Dependent Photon Emission from Organometal Halide Perovskite Nanocrystals Embedded in an Organic Matrix. *J. Phys. Chem. Lett*. **2015**, *6*, 446−450.

(42) Galkowski, K.; Mitioglu, A.; Miyata, A.; Plochocka, P.; Portugall, O.; Eperon, G. E.; Wang, J. T.-W.; Stergiopoulos, T.; Stranks, S. D.; Snaith, H. J.; Nicholas, R. J. Determination of the Exciton Binding Energy and Effective Masses for Methylammonium and Formamidinium Lead Tri-Halide Perovskite Semiconductors. *Energy Environ. Sci.* **2016** (DOI: 10.1039/c5ee03435c)

(43) Hirasawa, M.; Ishihara, T.; Goto, T.; Uchida, K.; Miura, N. Magneto absorption of the Lowest Exciton in Perovskite-Type Compound $(CH_3NH_3)PbI_3$. *Physica B: Condensed Matter* **1994**, *201*, 427-430.

(44) Tanakaa, K.; Takahashia, T.; Bana, T.; Kondoa, T.; Uchidab, K.; Miurab, N. Comparative Study on the Excitons in Lead-Halide-Based Perovskite type Crystals $CH_3NH_3PbBr_3$, $CH_3NH_3PbI_3$. *Solid State Commun.* **2003**, *127*, 619-623.

TOC FIGURE